Received: 12 May 2021 | Accepted: 19 July 2021

DOI: 10.1111/bpa.13011

Brain Pathology

RESEARCH ARTICLE

Integrated genotype–phenotype analysis of long-term epilepsy-associated ganglioglioma

Yujiao Wang[1] | **Leiming Wang**[1] | **Ingmar Blümcke**[2] | **Weiwei Zhang**[1] | **Yongjuan Fu**[1] | **Yongzhi Shan**[3,4] | **Yueshan Piao**[1,4] | **Guoguang Zhao**[3,4]

[1]Department of Pathology, Xuanwu Hospital, Capital Medical University, Beijing, China

[2]Department of Neuropathology, University Hospital Erlangen, Erlangen, Germany

[3]Department of Neurosurgery, Xuanwu Hospital, Capital Medical University, Beijing, China

[4]Clinical Research Center for Epilepsy Capital Medical University, Beijing, China

Correspondence
Yueshan Piao, Department of Pathology, Xuanwu Hospital, Capital Medical University, Beijing, China.
Email: yueshanpiao@126.com

Guoguang Zhao, Department of Neurosurgery, Xuanwu Hospital, Capital Medical University, Beijing, China.
Email: ggzhao@vip.sina.com.

Funding information
This work was supported by National Natural Science Foundation of China (Grant No. 82030037, No. 81871009, No. 81801288); Beijing Nova program (Grant No. Z201100006820149); Beijing Municipal Science and Technology Commission (Grant No. Z161100000516008) and Beijing Hospitals Authority Youth Programme (Grant No. QML20190805)

Abstract

The *BRAF p.V600E* mutation is the most common genetic alteration in ganglioglioma (GG). Herein, we collected a consecutive series of 30 GG specimens from Xuanwu Hospital in order to corroborate the genetic landscape and genotype–phenotype correlation of this enigmatic and often difficult-to-classify epilepsy-associated brain tumor entity. All specimens with histopathologically confirmed lesions were submitted to targeted next-generation sequencing using a panel of 131 genes. Genetic alterations in three cases with histologically distinct tumor components, that is, GG plus pleomorphic xanthoastrocytoma (PXA), dysembryoplastic neuroepithelial tumor (DNT), or an oligodendroglioma (ODG)-like tumor component, were separately studied. A mean post-surgical follow-up time-period of 23 months was available in 24 patients. Seventy seven percent of GG in our series can be explained by genetic alterations, with *BRAF p.V600E* mutations being most prevalent (n = 20). Three additional cases showed *KRAS p.Q22R* and *KRAS p.G13R*, *IRS2* copy number gain (CNG) and a *KIAA1549-BRAF* fusion. When genetically studying different histopathology patterns from the same tumor we identified composite features with *BRAF p.V600E* plus *CDKN2A/B* homozygous deletion in a GG with PXA features, *IRS2* CNG in a GG with DNT features, and a *BRAF p.V600E* plus CNG of *chromosome* 7 in a GG with ODG-like features. Follow-up revealed no malignant tumor progression but nine patients had seizure recurrence. Eight of these nine GG were immunoreactive for CD34, six patients were male, five were *BRAF* wildtype, and atypical histopathology features were encountered in four patients, that is, ki-67 proliferation index above 5% or with PXA component. Our results strongly point to activation of the MAP kinase pathway in the vast majority of GG and their molecular-genetic differentiation from the cohort of low-grade pediatric type diffuse glioma remains, however, to be further clarified. In addition, histopathologically distinct tumor components accumulated different genetic alterations suggesting collision or composite glio-neuronal GG variants.

KEYWORDS
BRAF p.V600E, dysembryoplastic neuroepithelial tumor, epilepsy, ganglioglioma, MAP kinase signaling pathway, pleomorphic xanthoastrocytoma

1 | INTRODUCTION

Ganglioglioma (GG) is a slow-growing glio-neuronal neoplasm consisting of both, differentiated neurons and glial cell elements. GG also represents the most frequent entities of low-grade epilepsy-associated tumors (LEAT) (1–4). Glial cell elements typically comprise astrocytes, although oligodendroglial components have also been described (5, 6). The most common location for this neoplasm is the temporal lobe, and GG appears more commonly in children and young adults with early-onset focal epilepsy (6, 7). Currently, the most successful treatment option in GG is neurosurgical resection with almost no tumor recurrence (2, 8) or seizure relapse during a postsurgical follow-up period of 5 years (9). Histopathologically, most GG are considered as World Health Organization (WHO) grade I. Some GG with anaplastic features are considered WHO grade III (4, 10, 11). Anaplastic changes in the glial component and a high ki-67 proliferation index may indicate aggressive behavior and a less favorable prognosis (12, 13). At present, no criteria for a GG WHO grade II were established (1, 4).

The *BRAF-V600E* mutation is the most common genetic alteration in GG occurring in 20%-60% of published cases (14–18). Its pathogenetic impact in epilepsy-associated tumors was recently addressed following *in utero* electroporation into embryonic mice (19). Transfected animals developed a GG-specific histopathology and CD34-immunreactivity phenotype, when glial precursor cells were expressing mutated BRAF. A seizure phenotype was observed in all animals with *BRAFV600E*-transfected neuronal precursor cells, and experimentally confirmed as REST-mediated pathomechanism (19). The *BRAF-V600E* mutation is not specific to GG, however. It has been detected first in malignant melanomas (20) as well as in pleomorphic xanthoastrocytoma (PXA). PXA is best described, however, with a genetic profile of *V600E*-mutant *BRAF* in addition to a homozygous deletion of *CDKN2A*/*B* (p16) (14, 21). Moreover, several studies have indicated a rare tumor composed of GG and PXA components, with fewer than 20 cases reported (22). Genetic alterations commonly described in diffuse glioma, that is, astrocytoma, oligodendroglioma (ODG),or glioblastoma do not play a role in GG or other LEAT, including *IDH1R132H* mutation, *1p*/*19q* co-deletions and *ATRX* mutations (4, 23, 24). More refined clinico-pathological and genetic studies will be necessary, therefore, to characterize those GG with unfavorable outcome, that is, seizure relapse, tumor regrowth, or malignant transformation, in order to improve clinical management of patients with chronic focal epilepsy and brain tumors. In our study, we characterized the genetic signature of 30 consecutive GG to be further integrated with clinical data and pathological features.

2 | MATERIALS AND METHODS

2.1 | Patients tissue

All 30 cases of GG received surgical treatment in the Department of Neurosurgery of Xuanwu Hospital, Capital Medical University, spanning the years 2014 to 2020. A full evaluation was conducted on all patients, including clinical examination, imaging inspection, and pathological diagnosis. Histopathological findings were systematically reviewed by two experienced neuropathologists according to the WHO classification scheme from 2016, including a panel of immunohistochemical markers. Histopathologically distinct tumor components were included in our research, that is, GG plus PXA, dysembryoplastic neuroepithelial tumor (DNT), ODG-like tumor. GG with a ki-67 proliferation index above 5% or GG with an additional PXA component were regarded as tumors with atypical histopathology features (Table 1).

2.2 | Genomic DNA extraction

Tumor areas were circled in hematoxylin and eosin-stained slides under the microscope. The formalin-fixed paraffin-embedded (FFPE) tumor tissue was matched with the corresponding hematoxylin-eosin (HE) stained section, and the tumor area was manually microdissected. According to the manufacturer's protocol, genetic DNA from human tumor tissues was extracted using a DNeasy Tissue kit (Qiagen, Hilden, Germany).

2.3 | Targeted next-generation sequencing

All FFPE tissue specimens with histopathologically confirmed lesions were submitted to targeted next-generation sequencing using a panel of 131 genes (see Table S1). Genetic alterations in three cases with histologically distinct tumor components, that is, GG plus PXA, DNT, ODG-like tumor, were separately studied. Sequencing libraries were prepared from genomic DNA by KAPA HyperPlus Library Preparation Kit (KAPA,

America, 006051-9-1/006077-7-1). The target region is captured by hybridizing the gDNA sample library with the probe. Moreover, the capture DNA library was amplified by KAPA HiFi HotStart ReadyMix. Sequencing was performed on NovaSeq 6000 according to the manufacturer's protocol. The average read depth of sequencing was 1000×. Single nucleotide variants (SNVs), gene fusion, copy number variations (CNVs), and chromosomal copy number alterations were analyzed. Base calls from Illumina NovaSeq 6000 were conducted to FASTQ files. The software fastp (v.2.20.0) was used for adapter trimming and filtering of low-quality bases. SNVs/InDels were called and annotated via VarDict (v.1.5.7) and InterVar. CNVs and fusions were analyzed by CNVkit (dx1.1) and factera (v1.4.4), respectively.

2.4 | Histological and immunohistochemical stainings

All tissue sections were dewaxed in xylene, dehydrated in a serial alcohol gradient, washed in PBS, and then stained with hematoxylin and eosin (H&E). Reticular fibers were visualized by Gomori's reticulin staining. Immunohistochemical staining was performed as previously described (25). After being blocked with 10% goat serum, the sections were sequentially incubated with a well-suited primary antibody and second antibody. Then these sections were processed by the polymer horseradish peroxidase (HRP) detection system [Polink-1HRP Broad Spectrum DAB Detection Kit, Golden Bridge International (GBI), Mukilteo, WA, USA]. The following primary antibodies were used: anti-BRAF V600E (Spring Bioscience, USA, monoclonal, clone VE1, 1:50), anti-CD34 (Zymed, USA, monoclonal, clone QBEnd 10, 1:50), anti-neurofilament protein (NF; OriGene, USA, monoclonal, clone 2F11, 1:200), anti- neuronal nuclear antigen (NeuN; Chemicon, USA, monoclonal, 1:4000), anti- glial fibrillary acidic protein (GFAP; OriGene, USA, monoclonal, clone UMAB129, 1:200), and anti-Ki67 (MIB-1; OriGene, USA, monoclonal, clone UMAB107, 1:200). Ki-67 proliferation index was defined by the percentage of ki-67-positive cells in the total cell population. The areas with the highest numbers of ki-67 labeled nuclei ("hotspots") were evaluated at 40 magnification of 10 microscopic fields.

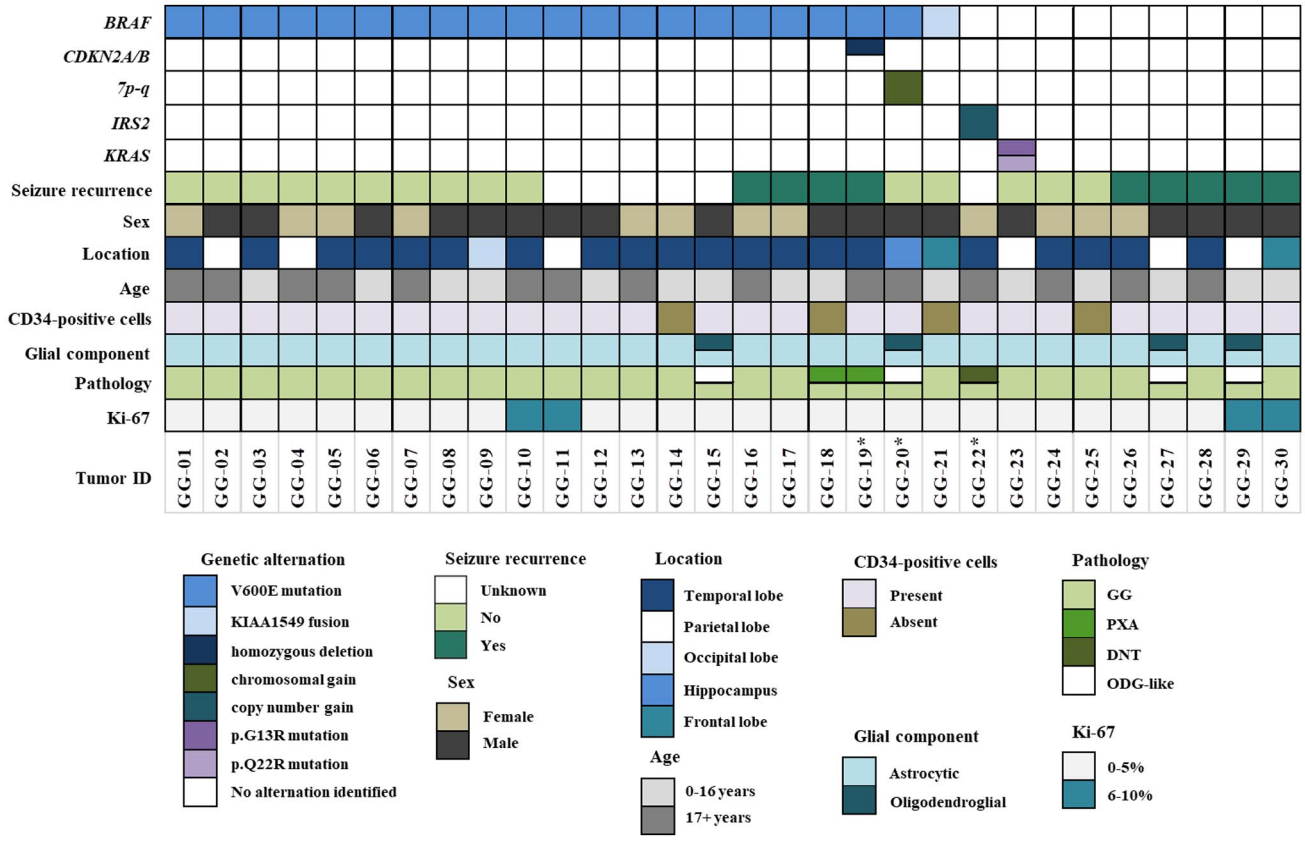

FIGURE 1 Summary table of genetic, clinical, and histological features in 30 GG. *The histopathology patterns, that is, GG plus PXA (GG-19), ODG-like tumor (GG-20) and DNT (GG-22), were identified and separately conducted with genomic profiling. The GG and PXA components both harbored *BRAF p.V600E* hotspot mutation, while the PXA component additionally showed homozygous deletion of *CDKN2A*/*B* in GG-19. Chromosome 7 gain was found in both GG and ODG-like components of GG-20, which also had identical single nucleotide variants-*BRAF p.V600E* hotspot mutation. Both the GG and DNT components revealed *IRS2* CNG in GG-22

2.5 | Postsurgical follow-up

Twenty-four patients were available for follow up until October 28, 2020 with a mean follow-up period of 23 months. Tumor recurrence or progression was assessed by magnetic resonance imaging (MRI). Seizure recurrence was assessed by electroencephalography (EEG) and clinical symptoms. The postoperative

TABLE 1 Summary of the clinico-pathologic features and molecular alterations in the patient cohort

Tumor ID	Seizure recurrence	Age/sex	Pathogenic genetic alterations identified	Chromosomal gains/losses	Pathology	Glial component	Ki-67
GG-01	No	26/F	BRAF p.V600E	None	GG	Astrocytic	2%–3%+
GG-02	No	26/M	BRAF p.V600E	None	GG	Astrocytic	5%+
GG-03	No	4/M	BRAF p.V600E	None	GG	Astrocytic	1%+
GG-04	No	29/F	BRAF p.V600E	None	GG	Astrocytic	<1%
GG-05	No	25/F	BRAF p.V600E	None	GG	Astrocytic	<1%
GG-06	No	2/M	BRAF p.V600E	None	GG	Astrocytic	1–2%+
GG-07	No	21/F	BRAF p.V600E	None	GG	Astrocytic	1%+
GG-08	No	3/M	BRAF p.V600E	None	GG	Astrocytic	5%+
GG-09	No	4/M	BRAF p.V600E	None	GG	Astrocytic	2%+
GG-10	No	19/M	BRAF p.V600E	None	GG	Astrocytic	10%+ (Partial)
GG-11	Unknown	21/M	BRAF p.V600E	None	GG	Astrocytic	10%+
GG-12	Unknown	2/M	BRAF p.V600E	None	GG	Astrocytic	1–2%+
GG-13	Unknown	20/F	BRAF p.V600E	None	GG	Astrocytic	2%+
GG-14	Unknown	2/F	BRAF p.V600E	None	GG	Astrocytic	1–2%+
GG-15	Unknown	11/M	BRAF p.V600E	None	GG + ODG-like	Astrocytic +oligodendroglial	5%+ (Partial)
GG-16	Yes	49/F	BRAF p.V600E	None	GG	Astrocytic	<1%
GG-17	Yes	6/F	BRAF p.V600E	None	GG	Astrocytic	1%+
GG-18	Yes	14/M	BRAF p.V600E	None	GG + PXA	Astrocytic	2%+
GG-19[a]	Yes	34/M	BRAF p.V600E	None	GG component	Astrocytic	<1%+
			BRAF p.V600E CDKN2A/B HD[b]	None	PXA component		
GG-20[a]	No	26/M	BRAF p.V600E	Chromosome 7 gain	GG component	Astrocytic + oligodendroglial	2%+
			BRAF p.V600E	Chromosome 7 gain	ODG-like component		
GG-21	No	12/M	KIAA1549-BRAF fusion	None	GG	Astrocytic	2%+
GG-22[a]	Unknown	35/F	IRS2 CNG	None	GG component	Astrocytic	<1%
			IRS2 CNG	None	DNT component		
GG-23	No	4/M	KRAS p.G13R KRAS p.Q22R	None	GG	Astrocytic	3%-5%
GG-24	No	33/F	None identified	None	GG	Astrocytic	5%+ (Partial)
GG-25	No	1/F	None identified	None	GG	Astrocytic	5%+ (Partial)
GG-26	Yes	63/F	None identified	None	GG	Astrocytic	<1%
GG-27	Yes	14/M	None identified	None	GG + ODG-like	Astrocytic + oligodendroglial	1%+
GG-28	Yes	23/M	None identified	None	GG	Astrocytic	<1%
GG-29	Yes	5/M	None identified	None	GG + ODG-like	Astrocytic + oligodendroglial	10%+ (Partial)
GG-30	Yes	2/M	None identified	None	GG	Astrocytic	7%−10%

[a]The histopathology patterns of GG and PXA components (GG-19), the GG and ODG-like components (GG-20), and the GG and DNT components (GG-22) were identified and conducted with respective genomic profiling.

[b]CDKN2A/B homozygous deletion.

seizure control was defined by Engel Class (Class I versus Class II, III and IV) (Engel J, Cascino GD, Nies PCV, Rasmussen TB, Ojemann LM. Outcome with respect to epileptic seizures. In: Engel J (editor) Surgical treatment of the epilepsies. NY:Raven Press, 1993).

Tumor location/ side	Extent of resection	Epilepsy onset (years)	Duration of epilepsy (years)	Tumor progression	Time to seizure recurrence (months)	Length of follow-up (months)
Temporal lobe/R	Gross total	14	12	No	23	23
Parietal lobe/L	Gross total	19	5	No	24	24
Temporal lobe/L	Gross total	1	3	No	25	25
Parietal lobe/L	Gross total	5	24	No	27	27
Temporal lobe/R	Subtotal	19	6	No	34	34
Temporal lobe/R	Gross total	1.67	0.33	No	34	34
Temporal lobe/L	Gross total	15	6	No	35	35
Temporal lobe/R	Gross total	0.42	2.58	No	35	35
Occipital lobe/R	Gross total	3.67	0.33	No	35	35
Temporal lobe/R	Gross total	18	1	No	19	19
Parietal lobe/R	Gross total	17	3	Unknown	Unknown	Unknown
Temporal lobe/L	Gross total	1.33	0.67	Unknown	Unknown	Unknown
Temporal lobe/L	Gross total	14	6	Unknown	Unknown	Unknown
Temporal lobe/R	Gross total	1.5	0.5	Unknown	Unknown	Unknown
Temporal lobe/R	Gross total	9	2	Unknown	Unknown	Unknown
Temporal lobe/L	Gross total	20	29	No	36	36
Temporal lobe/R	Subtotal	5.92	0.08	No	6	6
Temporal lobe/L	Gross total	8	6	No	36	36
Temporal lobe/R	Gross total	24	10	No	23	23
hippocampus/L	Gross total	22	4	No	23	23
Frontal lobe/R	Subtotal	10.5	1.5	No	5	5
Temporal lobe/R	Gross total	–	–	Unknown	Unknown	Unknown
Parietal lobe/R	Gross total	3.25	0.75	No	4	4
Temporal lobe/L	Gross total	32.92	0.08	No	22	22
Temporal lobe/L	Gross total	0.42	0.58	No	3	3
Temporal lobe/R	Subtotal	40	23	No	36	36
Parietal lobe/L	Subtotal	6	8	No	22	22
Temporal lobe/R	Gross total	4	19	No	2	2
Parietal lobe/L	Gross total	1	4	No	36	36
Frontal lobe/L	Gross total	1.92	0.08	No	3	3

TABLE 2 Clinical and histopathology features of 30 patients with GG

Characteristics	Total cohort (n = 30)	*BRAF p.V600E* (n = 20)	*BRAF wildtype* (n = 9)	*p*
Age (years), median (range)	16.5 (1–63)	19.5 (2–49)	14 (1–63)	0.6599
Male/female	18/12	12/8	5/4	1
Location				
Temporal lobe	20 (66.7%)	15 (75%)	5 (55.6%)	
Parietal lobe	6 (20%)	3 (15%)	3 (33.3%)	
Occipital lobe	1 (3.3%)	1 (5%)	0	
Frontal lobe	2 (6.7%)	0	1 (11.1%)	
hippocampus	1 (3.3%)	1 (5%)	0	
Epilepsy onset time (years), median (range)	8 (0.42–40)	11.5(0.42–24)	3.63 (0.42–40)	0.9624
Duration of Epilepsy (years), (mean ± SEM)	6.15 ± 1.47	6.08 ± 1.73	6.94 ± 3.24	0.8023
Seizure recurrence, yes: no (recurrence rate)[a]	9/15 (37.5%)	4/11 (26.7%)	5/3 (62.5%)	0.1793
Glial component				
Astrocytic	30 (100%)	20 (100%)	9 (100%)	
Astrocytic + oligodendroglial	4 (13.3%)	2 (10%)	2 (22.2%)	
Calcification	12 (36.7%)	9 (40%)	2 (22.2%)	
CD34-positive cells	27 (86.7%)	18 (90%)	8 (77.8%)	
Subpial CD34 spread	11 (36.7%)	9 (45%)	2 (22.2%)	
microvascular proliferation	20 (66.7%)	15 (75%)	5 (55.6%)	
Perivascular lymphocytes	2 (6.7%)	2 (10%)	0	
ki-67				
≤5%	26 (86.7%)	18 (90%)	7 (77.8%)	
6%−10%	4 (13.3%)	2 (10%)	2 (22.2%)	

[a]Exclude lost data.

2.6 | Statistical analysis

Data were analyzed using IBM SPSS version 23.0 and GraphPad Prism 6.02. The follow-up time was measured from the date of surgery to seizure recurrence or last follow-up. Univariate and multivariate analysis was done using Cox's proportional hazards analysis. Clinical and histological data of GG was performed using unpaired Student's *t*-test and Fisher's exact test. The *p*-value of less than 0.05 was considered significant.

3 | RESULTS

3.1 | Clinical features of patients with ganglioglioma

The median age of diagnosis was 16.5 years (range 1–63 years). Of these 30 cases, 18 were male, and 12 were female (male-to-female ratio, 1.5:1). Tumors were located most frequently in the temporal lobe (20/66.7%). Another six cases were located in the parietal lobe (20%), two in the frontal lobe (6.7%), one in the occipital lobe (3.3%), and one in the hippocampus (3.3%). Gross total resection was achieved in 25 patients, and subtotal resection was performed in 5 patients (Figure 1, Tables 1, and 2 and Table S2).

3.2 | Histopathological findings in ganglioglioma included into this series

All 30 GG revealed a combination of neuronal and glial cell elements. Neuronal components were characterized by enlarged dysmorphic ganglion cells, a lack of cyto-architectural organization, perimembraneous aggregation of Nissl substance, or occasionally presence of binucleated forms, or clustering of abnormal neurons not otherwise/anatomically explicable (6) (Figure 2). An astrocytic component was visible in all 30 cases. Two of these cases showed cellular pleomorphism and multinucleated cells, and were diagnosed as a combination of GG and PXA (Figure 3). In GG-18, the lesion consisted of two distinct neoplastic components. One component was marked by a proliferation of gangliocyte-like cells. The second component was composed of spindle cells, among which we also observed xanthomatoid cells with abundant cytoplasm. Both components showed either a zonation pattern, or they were randomly intermingled with each other. Light microscopy findings also revealed increased reticular fiber deposition in the PXA component (Figure 3). One other case additionally showed features with floating neurons surrounded by oligodendrocyte-like cells, and was diagnosed as a composite of GG

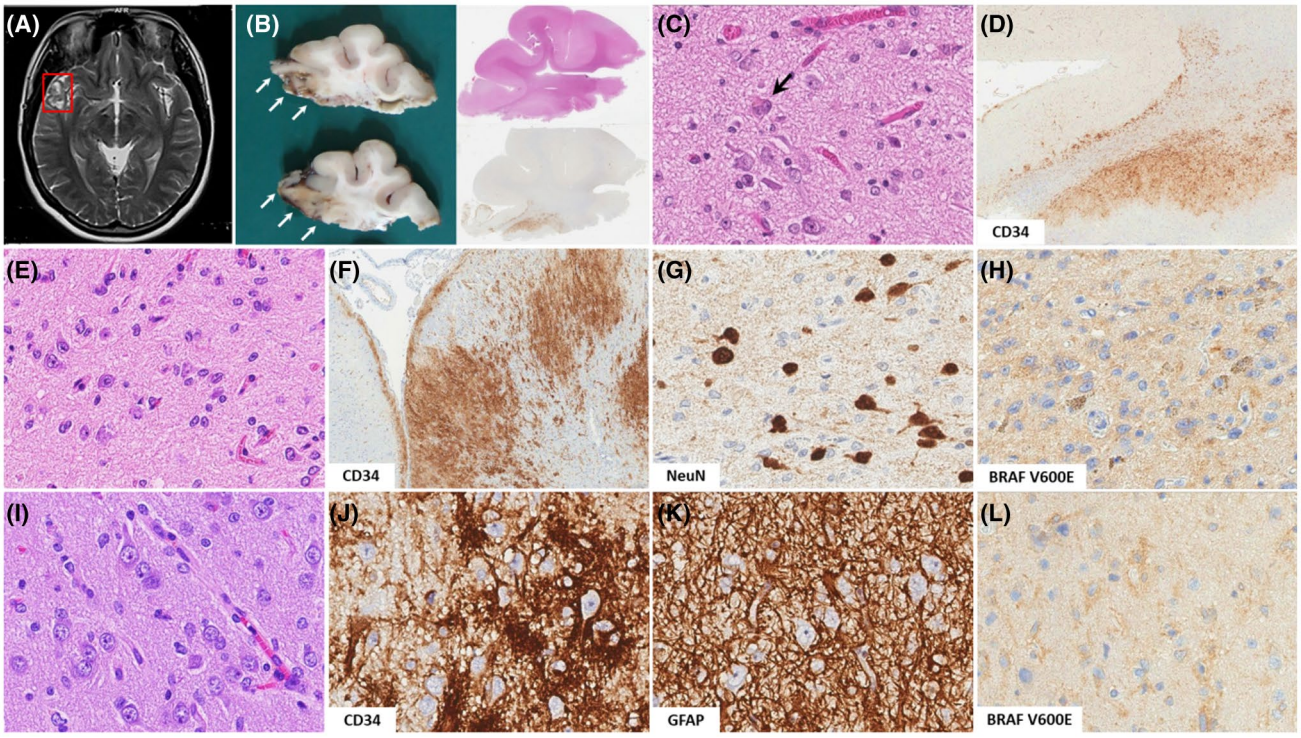

FIGURE 2 Histopathology findings in *BRAF p.V600E* mutated GG with postsurgical seizure control. (A–D) Magnetic resonance imaging image of a case with local signal abnormalities in the right anterior temporal lobe (A). Macroscopically, well-delineated brown lesion involving cortex and white matter was observed (B, white arrows). Microscopically, dysplastic neurons presented the binucleated form (C, black arrow), and CD34 immunostaining showed diffuse pattern along the lesion (B, D) (GG-01). (E–H) A GG with a characteristic glial-neuronal phenotype (E-HE), showed strong CD34 immunoreactivity with subpial spread (F), neuronal components (G) and positive BRAF V600E immunostaining (H) (GG-02). (I–L) A case with clustering of dysmorphic ganglion cells (I-HE) and astrocyte-element (K), had CD34-immunoreactive cell cluster (J) and positive BRAF V600E immunoreactivity (L) (GG-05)

and DNT (Figure 4). Four cases revealed clear cell elements, resembling ODG-like lesions (Figure 5). The CD34 staining was strongly positive in 26 cases (86.7%) and displayed a solitary, clustered or diffuse pattern (26, 27). Positive BRAF V600E immunostaining was observed in 20 of 30 specimens (66.7%), and was confirmed by sequencing in all cases (see below). Twenty-six cases had a ki-67 proliferation index below 5% (86.7%), compared to 4 cases with a ki-67 proliferation index above 5% (13.3%). No *IDH-1/2* mutations were identified in these cases by panel sequencing (see below). All histology features were summarized in Figures 2-5, Table 2 and Table S3.

3.3 | Genetic findings in ganglioglioma

Panel sequencing revealed genetic alterations in 23 tumors (77%; Table 1), with *BRAF p.V600E* mutations being most prevalent (n = 20). One additional tumor revealed a *KIAA1549-BRAF* fusion. In those nine GG lacking *BRAF* alterations, one tumor had two *KRAS* hotspot mutations (*KRAS p.Q22R and KRAS p.G13R*), and one tumor revealed an *IRS2* copy number gain (CNG). The remaining seven tumors did not contain any identifiable pathogenic alteration. When genetically studying different histopathology patterns from the same tumor, we identified composite features. The GG and PXA components of case GG-19 both harbored *BRAF p.V600E* hotspot mutation, while the PXA component also harbored concomitant *CDKN2A/B* homozygous deletion. *Chromosome 7* gain was found in both parts of GG-20 with GG and ODG-like features and a *BRAF p.V600E* mutation. Moreover, the GG and DNT region of GG-22 both revealed a copy-number gain of *IRS2* (Figure 1, Table 1, Tables S4 and S5 and Figure S1).

3.4 | Seizure recurrence in patients with ganglioglioma

Clinical analysis revealed no malignant tumor progression in our patient cohort. Postoperatively, 62.5% of patients (15/24) were utterly seizure-free (Engel's class I), but nine patients had postoperative seizure relapse as confirmed by EEG. Eight of these nine GG were immunoreactive for CD34. Six patients were male and three patients were female (male-to-female ratio, 2:1). Six GG were located in the temporal lobe. Four of the nine cases harbored a *BRAF p.V600E* mutation, and the remaining five cases were *BRAF* wildtype. Atypical histopathology features were encountered in six patients,

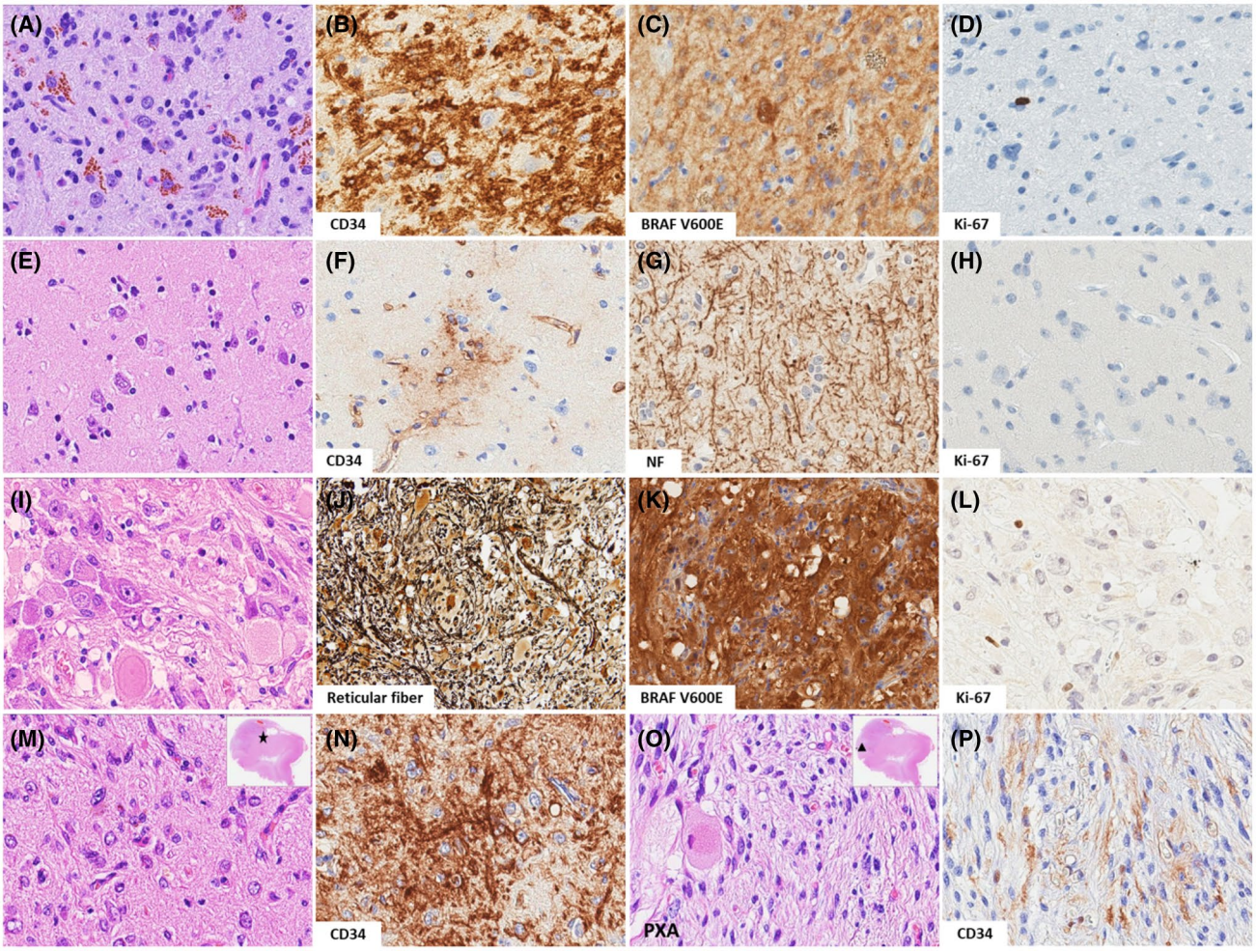

FIGURE 3 Histopathology findings in *BRAF p.V600E* mutated GG with seizure recurrence. (A–D) A GG with a characteristic glial-neuronal phenotype and hemosiderin deposition (A-HE), the strongly positive CD34 staining (B), positive BRAF V600E (C) immunoreactivity and low ki-67 proliferation index (D) in the lesion (GG-16). (E–H) A GG with a characteristic glial-neuronal phenotype (E-HE), the fine positive CD34 immunoreactivity (F), enriched neurofilament (G) and low ki-67 proliferation index (H) (GG-17). (I–L) A case with intermingled GG and PXA components (I-HE), increased reticular fiber deposition in PXA region (J), the strongly positive BRAF V600E (K) immunoreactivity and low ki-67 proliferation index (L) in the tumor lesion (GG-18). (M–P) A case with both GG component (M-HE, shown as the asterisk marked area in the upper right corner) and PXA component (O-HE, shown as a triangle marked area in the upper right corner) was conducted the genomic profiling respectively. The CD34 staining was diffusely positive in GG component (N), while displayed a fine pattern in PXA component (P) (GG-19)

that is, GG containing a ki-67 proliferation index above 5% or GG with an additional PXA component, four of which had a seizure recurrence ($p = 0.0474$*) (Table S6).

3.5 | Integrated analysis of genetic alterations, histological and clinical features

We compared the patients based on the presence of the *BRAF p.V600E* mutation (Tables 2 and 3). The median age of epilepsy onset was 11.5 years in *BRAF p.V600E* mutation vs. 3.63 years in *BRAF* wildtype. The interesting association of *BRAF p.V600E* mutation in GG of patients with later seizure onset did not reach, however, statistical significance ($p = 0.9624$). We could not observe any association between *BRAF p.V600E* mutation and histopathology features in our tumor cohort (Table 2; Figures 2-5). Furthermore, there was no difference in seizure recurrence between patients with GG carrying a *BRAF p.V600E* mutation or GG with *BRAF wildtype* ($p = 0.1793$). This was confirmed by cox's proportional hazards analysis [Univariate: HR=0.416 (0.104–1.661), $p = 0.215$; Multivariate: HR=0.376 (0.034–4.159), $p = 0.425$] (Table 3).

4 | DISCUSSION

A comprehensive genotype–phenotype analysis linking genomic data with clinical and histological features proved helpful to obtain a reliable classification scheme in pediatric low-grade glioma (pLGG) (28).

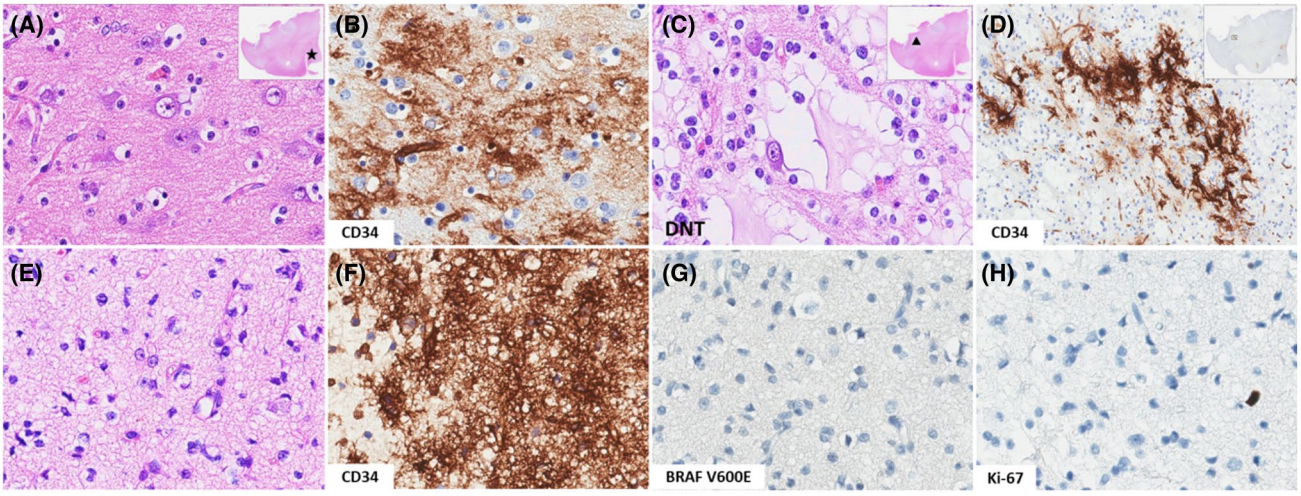

FIGURE 4 Histopathology findings in genetically positive, none-*BRAF p.V600E* mutated GG. (A–D) A case with both, GG (A-HE, shown as the asterisk marked area in the upper right corner) and DNT components (C-HE, shown as a triangle marked area in the upper right corner) (GG-22) were detected both harboring *IRS2* CNG in two components, respectively. The CD34 staining was diffusely positive in GG component (B). Floating neuron is interspersed in a mucoid matrix surrounded by oligodendrocyte-like cells (C). And scanty positive CD34 immunoreactivity was observed in DNT component (D). (E–H) A GG with several neurons scattered in glial cells (E-HE), the positive CD34 immunoreactivity (F), negative BRAF V600E staining (G) and low ki-67 proliferation index (H). The tumor harbored *KRAS p.Q22R* and *KRAS p.G13R* mutations (GG-23)

The histopathology-based selection of 30 tumors with a glio-neuronal phenotype and classification according to WHO criteria as GG revealed two genetically different subtypes. A majority of 23 GG was defined by alterations in the MAPK pathway including *BRAF p.V600E* and *KRAS* mutations, *IRS2* CNG, or a *KIAA1549-BRAF* fusion. Genetic alterations in a second minor group of 7 tumors remained yet undetermined (23%). Such a comprehensive genotype–phenotype analysis will also be a pre-requisite for any further molecular characterization, that is, using DNA methylation profiling (29), in order to define clinically meaningful categories.

A *BRAF p.V600E* mutation is the most common gene mutation in published GG series (20%-60%), and results in substitution of valine by glutamic acid at codon 600 (*V600E*) in the activation segment of the kinase (30). *V600E*-mutant BRAF protein can be immunohistochemically detected in dysplastic ganglion cells of GG as well as in glial cells and cells of intermediate differentiation (4, 31). Koh and coworkers experimentally confirmed the impact of a *BRAF p.V600E* hotspot mutation when transfected in neuronal and glial precursor cell lineages during murine brain development (19). These effects could be addressed further experimentally and confirmed their functional impact for tumorigenesis when targeted in glial cells and epileptogenesis when targeted in neurons. Indeed, *BRAF p.V600E* mutation was previously associated with a worse recurrence-free survival in pediatric GG (4, 32), but appeared not related to long-term seizure relapse (32). Similarly, *BRAF p.V600E* mutation showed no significant correlation with seizure recurrence in our cohort, but none of our patients suffered from post-surgical tumor progression during the available clinical follow-up period of 23 months. A *KIAA1549-BRAF* fusion results in the *BRAF* kinase domain's constitutive activity and hyperactivation of the MAPK pathway in a similar pattern as *BRAF p.V600E* mutation (33). Hawkins et al. reported that pLGG with a *KIAA1549-BRAF* fusion have excellent overall survival and rarely progress (24, 34). Despite the different cohort described in the latter study, the GG with *KIAA1549-BRAF* fusion also showed no tumor progression or seizure recurrence in our cohort. Less common variants such as *KRAS* mutations (*KRAS p.Q22R* and *KRAS p.G13R*) were also detected in one of our GG samples, wand hich has been identified also in a previous study (35). KRAS can activate the same Ras-Raf-MEK-ERK signaling pathway as *BRAF p.V600E* mutation (36–38), suggesting that *KRAS* mutations also drive GG tumorigenesis by MAP-kinase pathway activation.

Combined GG with PXA is an extremely rare brain tumor with a relatively benign course (22, 39). Our histological analyses revealed two tumors with GG and PXA components, and both with a low ki-67 proliferation index. Consistent with previous reports (22), *BRAF p.V600E* mutation was observed in both GG and PXA components, suggesting that both cell lineages may share a common cellular origin. Genetic alterations could be studied separately for both components in one case and observed a concurrent *CDKN2A*/*B* homozygous deletion only in the PXA component. It is for the first time, that distinct genetic alterations can be reported in two different components of one tumor, that is, GG with PXA. Mixed GG and DNT variants were first described in 1998 (40). Genomic profiling pointed

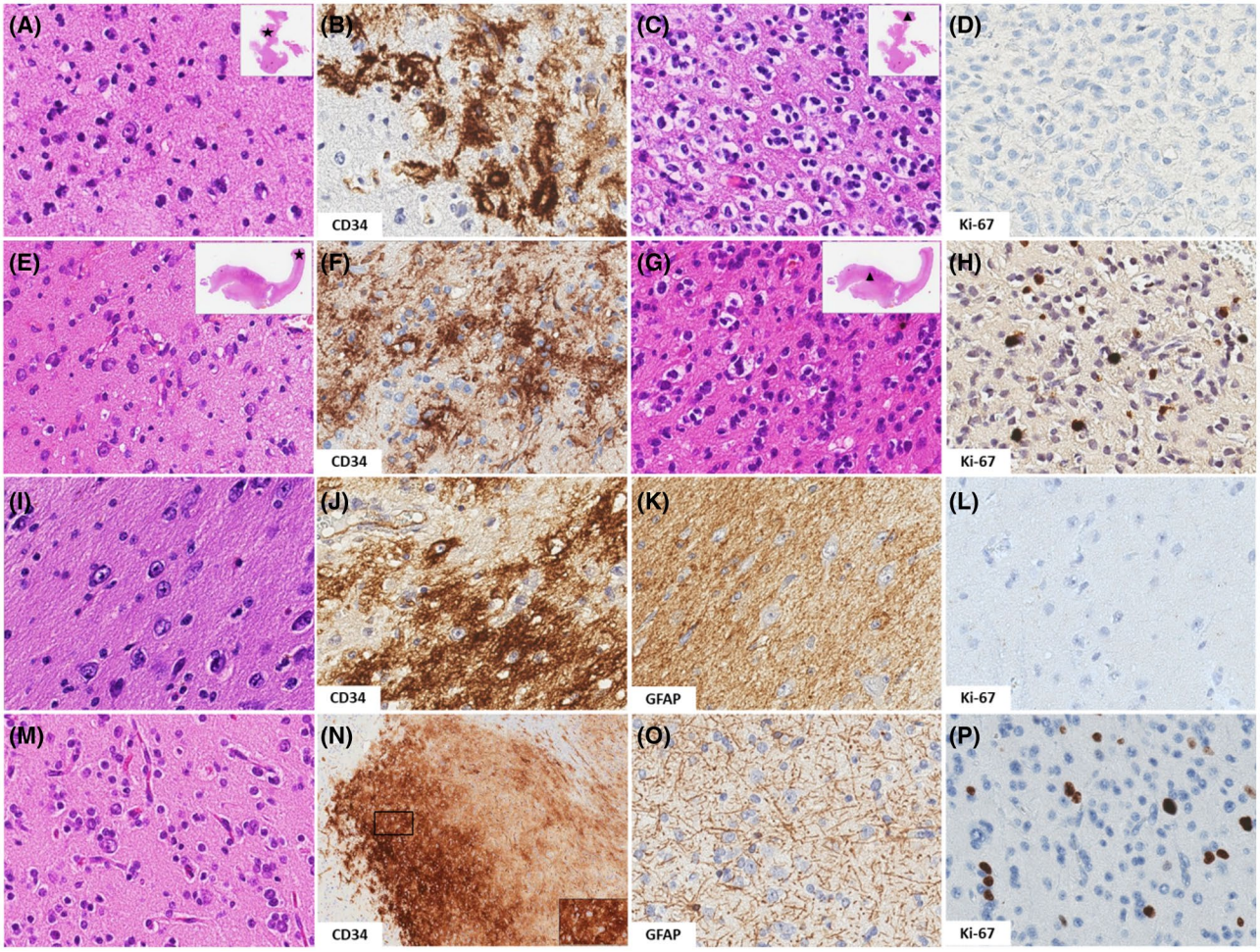

FIGURE 5 Histopathology findings in genetically negative tested GG with seizure recurrence. (A–D) (GG-27), (E–H) (GG-29) The GG with a characteristic astrocytic component (A-HE, E-HE, shown as the asterisk marked area in the upper right corner) and oligodendroglial component (ODG-like tumor) (C-HE, G-HE, shown as a triangle marked area in the upper right corner), CD34 immunoreactivity (B, F). The ki-67 proliferation index was below 5% (D) in GG-27, but above 5% (H) in GG-29. (I-L) (GG-28), (M-P) (GG-30) The GG with a characteristic glial-neuronal phenotype (I-HE, M-HE), CD34 immunoreactivity (J, N) and predominant astroglial component (K, O). The ki-67 proliferation index was below 5% (L) in GG-28, but above 5% (P) in GG-30

TABLE 3 Univariate and multivariate Cox analyses of 30 GG for Sex, CD34 expression, glial component, Ki-67, extent of resection and *BRAF V600E*

	Univariate			Multivariate		
Variables	**HR**	**95.0% CI**	***p***	**HR**	**95.0% CI**	***p***
Sex	0.622	0.155–2.505	0.504	0.133	0.008–2.277	0.164
CD34 expression	1.439	0.171–12.122	0.738	1.872	0.114–30.686	0.660
Glial component	1.211	0.247–5.931	0.813	0.213	0.015–3.018	0.253
Ki-67	1.474	0.292–7.442	0.639	1.378	0.090–21.066	0.818
Extent of resection	0.548	0.136–2.211	0.398	.286	0.016–5.135	0.396
BRAF V600E	0.416	0.104–1.661	0.215	.376	0.034–4.159	0.425

to *FGFR1* alterations as most prominent feature in DNT, with an approximate prevalence of 58.1%–82% (4). We detected *IRS2* CNG in a GG with DNT features, which has not been reported in mixed GG and DNT. Insulin receptor substrate (IRS) is a direct target of insulin-like growth factor receptor 1 (IGF-1R) and insulin receptor

(IR) signaling, and plays a crucial role in the transduction of IGF-1R/IR signaling to RAS/RAF/MEK/ERK (MAPK) and PI3K/AKT pathways, leading to cell proliferation and survival (36, 41, 42). Huang et al. demonstrated the percentage of *IRS2* CNG in colorectal cancer is higher than in any other tumor types (36). There are only few *IRS2* mutation studies in brain tumor research. Recently, Eyler et al. indicated copy number amplifications of the *IRS1* or *IRS2* loci in primary glioblastomas and which may underlie the inefficacy of targeted therapies in this disease (43). But the mechanism of *IRS2* CNG in GG with DNT features needs further investigation. Moreover, chromosomal copy number analysis revealed a gain of chromosome 7 as most common structural chromosomal alteration in GG (44). The structural and numerical abnormalities can differ, however, from case to case (45). No chromosomal gains or losses were identified in our other 29 cases, indicating that most GG of our histopathologically selected cohort are genetically homogeneous (simple) tumors.

The overwhelming presence of MAPK-pathway activation in our series of GG surge the discussion of how to best differentiate these tumors from pediatric low-grade glioma. *KIAA1549-BRAF* fusion and *BRAF p.V600E* mutations account for almost two-thirds of 1000 pLGG (28). pLGG appear to comprise two clinical subgroups; clinically benign tumors are characterized rather by rearrangements, that is, *KIAA1549-BRAF* fusion, and those of higher risk were SNV-driven, that is, by *BRAF p.V600E* mutations. Histopathology features in low-grade epilepsy-associated tumors are nonetheless often difficult to classify and result in a considerable disagreement amongst neuropathologists (6). In our cohort, the SNV-driven component prevailed but an unfavorable clinical signature was present in only 9 patients manifesting as post-surgical seizure relapse. We encountered no tumor progression or malignant transformation. Seizure relapse may result from various factors, that is, incomplete neurosurgical resection, but our cases could be histopathologically associated also with atypical features, that is, PXA component or a higher ki-67 proliferation index.

Panel-based targeted sequencing is widely used nowadays for routine molecular diagnostics, but limited data are available about the diagnostic yield and sensitivity when using epilepsy surgery samples with abnormal cells admixed with preexisting normal neuroepithelial cells (46). The lack of identifiable genetic alterations in our cohort may also be due to the limitation of the chosen gene panel. Future research should expand the cohort and extend molecular-genetic investigations to identify the pathogenic cause in all LEAT irrespective of their histopathological phenotypes.

ACKNOWLEDGMENTS

We thank Ze-liang Hu, Li-hong Zhao, and Wei-min Wang for their technical assistance. We kindly thank Ingmar Blümcke for careful guidance.

CONFLICT OF INTEREST

The authors state that they have no conflicts of interest.

AUTHOR CONTRIBUTIONS

Yujiao Wang, Weiwei Zhang, Yongzhi Shan: collected, analyzed and interpreted the clinical and imaging data. Yujiao Wang, Leiming Wang, and Yongjuan Fu: analyzed the immunohistochemistry results. Yujiao Wang, Ingmar Blümcke, Yue-Shan Piao, and Guoguang Zhao: contributed to analysis of the diagnostic results and discussion. Yujiao Wang, Ingmar Blümcke, Yue-Shan Piao, and Guoguang Zhao: wrote and revised the paper.

ETHICAL APPROVAL

All patient protocols were authorized by the Ethics Committee of Xuanwu Hospital, Capital Medical University (approval number [2021]068), and conformed to the Declaration of Helsinki's ethical principles. Written informed consent was acquired from all human subjects.

DATA AVAILABILITY STATEMENT

The datasets used and analyzed in the current study are available from the corresponding author on reasonable request.

ORCID

Leiming Wang https://orcid.org/0000-0002-8257-0175
Ingmar Blümcke https://orcid.org/0000-0001-8676-0788
Yueshan Piao https://orcid.org/0000-0001-6081-1129

REFERENCES

1. Blümcke I, Aronica E, Becker A, Capper D, Coras R, Honavar M, et al. Low-grade epilepsy-associated neuroepithelial tumours - the 2016 WHO classification. Nat Rev Neurol. 2016;12(12):732–40.
2. Luyken C, Blümcke I, Fimmers R, Urbach H, Elger CE, Wiestler OD, et al. The spectrum of long-term epilepsy-associated tumors: long-term seizure and tumor outcome and neurosurgical aspects. Epilepsia. 2003;44(6):822–30.
3. Thom M, Blümcke I, Aronica E. Long-term epilepsy-associated tumors. Brain Pathol. 2012;22(3):350–79.
4. Slegers RJ, Blümcke I. Low-grade developmental and epilepsy associated brain tumors: a critical update 2020. Acta Neuropathol Commun. 2020;8(1):27.
5. Louis DN, Perry A, Reifenberger G, von Deimling A, Figarella-Branger D, Cavenee WK, et al. The 2016 World Health Organization classification of tumors of the central nervous system: a summary. Acta Neuropathol. 2016;131(6):803–20.
6. Blümcke I, Coras R, Wefers AK, Capper D, Aronica E, Becker A, et al. Review: Challenges in the histopathological classification of ganglioglioma and DNT: microscopic agreement studies and a preliminary genotype-phenotype analysis. Neuropathol Appl Neurobiol. 2019;45(2):95–107.
7. Blümcke I, Spreafico R, Haaker G, Coras R, Kobow K, Bien CG, et al. Histopathological findings in brain tissue obtained during epilepsy surgery. N Engl J Med. 2017;377(17):1648–56.
8. Luyken C, Blümcke I, Fimmers R, Urbach H, Wiestler OD, Schramm J. Supratentorial gangliogliomas: histopathologic

grading and tumor recurrence in 184 patients with a median follow-up of 8 years. Cancer. 2004;101(1):146–55.
9. Lamberink HJ, Otte WM, Blümcke I, Braun KPJ. Seizure outcome and use of antiepileptic drugs after epilepsy surgery according to histopathological diagnosis: a retrospective multicentre cohort study. Lancet Neurol. 2020;19(9):748–57.
10. Mallick S, Benson R, Melgandi W, Giridhar P, Rath GK. Impact of surgery, adjuvant treatment, and other prognostic factors in the management of anaplastic ganglioglioma. Child's Nervous System. 2018;34(6):1207–13.
11. Majores M, von Lehe M, Fassunke J, Schramm J, Becker AJ, Simon M. Tumor recurrence and malignant progression of gangliogliomas. Cancer. 2008;113(12):3355–63.
12. Romero-Rojas AE, Diaz-Perez JA, Chinchilla-Olaya SI, Amaro D, Lozano-Castillo A, Restrepo-Escobar LI. Histopathological and immunohistochemical profile in anaplastic gangliogliomas. Neurocirugia. 2013;24(6):237–43.
13. Schittenhelm J, Reifenberger G, Ritz R, Nägele T, Weller M, Pantazis G, et al. Primary anaplastic ganglioglioma with a small-cell glioblastoma component. Clin Neuropathol. 2008;27(2):91–5.
14. Chappé C, Padovani L, Scavarda D, Forest F, Nanni-Metellus I, Loundou A, et al. Dysembryoplastic neuroepithelial tumors share with pleomorphic xanthoastrocytomas and gangliogliomas BRAF(V600E) mutation and expression. Brain Pathol. 2013;23(5):574–83.
15. Dougherty MJ, Santi M, Brose MS, Ma C, Resnick AC, Sievert AJ, et al. Activating mutations in BRAF characterize a spectrum of pediatric low-grade gliomas. Neuro Oncol. 2010;12(7):621–30.
16. Zhang J, Wu G, Miller CP, Tatevossian RG, Dalton JD, Tang B, et al. Whole-genome sequencing identifies genetic alterations in pediatric low-grade gliomas. Nat Genet. 2013;45(6):602–12.
17. Fukuoka K, Mamatjan Y, Tatevossian R, Zapotocky M, Ryall S, Stucklin AG, et al. Clinical impact of combined epigenetic and molecular analysis of pediatric low-grade gliomas. Neuro-oncology. 2020;22(10):1474–83.
18. Niestroj LM, May P, Artomov M, Kobow K, Coras R, Pérez-Palma E, et al. Assessment of genetic variant burden in epilepsy-associated brain lesions. Eur J Hum Genet. 2019;27(11):1738–44.
19. Koh HY, Kim SH, Jang J, Kim H, Han S, Lim JS, et al. BRAF somatic mutation contributes to intrinsic epileptogenicity in pediatric brain tumors. Nat Med. 2018;24(11):1662–8.
20. Davies H, Bignell GR, Cox C, Stephens P, Edkins S, Clegg S, et al. Mutations of the BRAF gene in human cancer. Nature. 2002;417(6892):949–54.
21. Phillips JJ, Gong H, Chen K, Joseph NM, van Ziffle J, Bastian BC, et al. The genetic landscape of anaplastic pleomorphic xanthoastrocytoma. Brain Pathol. 2019;29(1):85–96.
22. Cicuendez M, Martinez-Saez E, Martinez-Ricarte F, Asanza EC, Sahuquillo J. Combined pleomorphic xanthoastrocytoma-ganglioglioma with BRAF V600E mutation: case report. J Neurosurg Pediatr. 2016;18(1):53–7.
23. Brat DJ, Verhaak RG, Aldape KD, Yung WK, Salama SR, Cooper LA, et al. Comprehensive, integrative genomic analysis of diffuse lower-grade gliomas. N Engl J Med. 2015;372(26):2481–98.
24. Ryall S, Tabori U, Hawkins C. Pediatric low-grade glioma in the era of molecular diagnostics. Acta Neuropathol Commun. 2020;8(1):30.
25. Piao YS, Lu DH, Chen L, Liu J, Wang W, Liu L, et al. Neuropathological findings in intractable epilepsy: 435 Chinese cases. Brain Pathol. 2010;20(5):902–8.
26. Blümcke I, Giencke K, Wardelmann E, Beyenburg S, Kral T, Sarioglu N, et al. The CD34 epitope is expressed in neoplastic and malformative lesions associated with chronic, focal epilepsies. Acta Neuropathol. 1999;97(5):481–90.
27. Blümcke I, Aronica E, Urbach H, Alexopoulos A, Gonzalez-Martinez JA. A neuropathology-based approach to epilepsy surgery in brain tumors and proposal for a new terminology use for long-term epilepsy-associated brain tumors. Acta Neuropathol. 2014;128(1):39–54.
28. Ryall S, Zapotocky M, Fukuoka K, Nobre L, Guerreiro Stucklin A, Bennett J, et al. Integrated molecular and clinical analysis of 1,000 pediatric low-grade gliomas. Cancer Cell. 2020;37(4):569–83.e5.
29. Capper D, Jones DTW, Sill M, Hovestadt V, Schrimpf D, Sturm D, et al. DNA methylation-based classification of central nervous system tumours. Nature. 2018;555(7697):469–74.
30. Liu H, Nazmun N, Hassan S, Liu X, Yang J. BRAF mutation and its inhibitors in sarcoma treatment. Cancer Med. 2020;9(14):4881–96.
31. Koelsche C, Wohrer A, Jeibmann A, Schittenhelm J, Schindler G, Preusser M, et al. Mutant BRAF V600E protein in ganglioglioma is predominantly expressed by neuronal tumor cells. Acta Neuropathol. 2013;125(6):891–900.
32. Dahiya S, Haydon DH, Alvarado D, Gurnett CA, Gutmann DH, Leonard JR. BRAF(V600E) mutation is a negative prognosticator in pediatric ganglioglioma. Acta Neuropathol. 2013;125(6):901–10.
33. Maraka S, Janku F. BRAF alterations in primary brain tumors. Discov Med. 2018;26(141):51–60.
34. Hawkins C, Walker E, Mohamed N, Zhang C, Jacob K, Shirinian M, et al. BRAF-KIAA1549 fusion predicts better clinical outcome in pediatric low-grade astrocytoma. Clin Cancer Res. 2011;17(14):4790–8.
35. Pekmezci M, Villanueva-Meyer JE, Goode B, Van Ziffle J, Onodera C, Grenert JP, et al. The genetic landscape of ganglioglioma. Acta Neuropathol Commun. 2018;6(1):47.
36. Huang F, Chang H, Greer A, Hillerman S, Reeves KA, Hurlburt W, et al. IRS2 copy number gain, KRAS and BRAF mutation status as predictive biomarkers for response to the IGF-1R/IR inhibitor BMS-754807 in colorectal cancer cell lines. Mol Cancer Ther. 2015;14(2):620–30.
37. Drosten M, Barbacid M. Targeting the MAPK pathway in KRAS-driven tumors. Cancer Cell. 2020;37(4):543–50.
38. Nussinov R, Tsai CJ, Jang H. Does Ras activate Raf and PI3K allosterically? Front Oncol. 2019;9:1231.
39. Sugita Y, Irie K, Ohshima K, Hitotsumatsu T, Sato O, Arimura K. Pleomorphic xanthoastrocytoma as a component of a temporal lobe cystic ganglioglioma: a case report. Brain Tumor Pathol. 2009;26(1):31–6.
40. Hirose T, Scheithauer BW. Mixed dysembryoplastic neuroepithelial tumor and ganglioglioma. Acta Neuropathol. 1998;95(6):649–54.
41. Degirmenci U, Wang M, Hu J. Targeting aberrant RAS/RAF/MEK/ERK signaling for cancer therapy. Cells. 2020;9(1):198.
42. Guo S. Insulin signaling, resistance, and the metabolic syndrome: insights from mouse models into disease mechanisms. J Endocrinol. 2014;220(2):T1–t23.
43. Eyler CE, Matsunaga H, Hovestadt V, Vantine SJ, van Galen P, Bernstein BE. Single-cell lineage analysis reveals genetic and epigenetic interplay in glioblastoma drug resistance. Genome Biol. 2020;21(1):174.
44. Hoischen A, Ehrler M, Fassunke J, Simon M, Baudis M, Landwehr C, et al. Comprehensive characterization of genomic aberrations in gangliogliomas by CGH, array-based CGH and interphase FISH. Brain Pathol. 2008;18(3):326–37.
45. Prabowo AS, van Thuijl HF, Scheinin I, Sie D, van Essen HF, Iyer AM, et al. Landscape of chromosomal copy number aberrations in gangliogliomas and dysembryoplastic neuroepithelial tumours. Neuropathol Appl Neurobiol. 2015;41(6):743–55.
46. Blümcke I, Coras R, Busch RM, Morita-Sherman M, Lal D, Prayson R, et al. Toward a better definition of focal cortical dysplasia: An iterative histopathological and genetic agreement trial. Epilepsia. 2021;62(6):1416–28.

SUPPORTING INFORMATION

Additional supporting information may be found online in the Supporting Information section.

FIGURE S1 Snapshots of genetic alterations identified in the 30 gangliogliomas. (A) GG with *BRAF p.V600E* mutation. (B) Composite features with *BRAF p.V600E* plus *CDKN2A*/*B* homozygous deletion in a GG with PXA features (GG-19). (C) *BRAF p.V600E* plus gain of *chromosome 7* in a GG with ODG-like features (GG-20). (D) GG with KIAA1549-BRAF fusion (GG-21). (E) *IRS2* copy number gain in a GG with DNT features (GG-22). (F) GG with *KRAS p.Q22R*, *KRAS p.G13R* mutation (GG-23)

TABLE S1 Targeted next-generation sequencing using a panel of 131 genes

TABLE S2 Clinical features of the 30 patients with ganglioglioma

TABLE S3 Histologic features of the 30 patients with ganglioglioma

TABLE S4 molecular characteristics of the 30 patients with ganglioglioma

TABLE S5 Chromosomal copy number alterations identified in the 30 ganglioglioma

TABLE S6 Clinical and histopathology features of 30 patients with ganglioglioma

How to cite this article: Wang Y, Wang L, Blümcke I, Zhang W, Fu Y, Shan Y, et al. Integrated genotype–phenotype analysis of long-term epilepsy-associated ganglioglioma. Brain Pathol. 2022;32:e13011. https://doi.org/10.1111/bpa.13011